THERMAL ANALYSIS OF PROPOSED HEAT SINK DESIGN UNDER NATURAL CONVECTION FOR THE THERMAL MANAGEMENT OF ELECTRONICS

by

Numan HABIB[a], Muftooh Ur Rehman SIDDIQI[a*], and Muhammad TAHIR[b]

[a] Mechanical, Biomedical, and Design Engineering Department, School of Engineering and Technology, Aston University, Birmingham, UK
[b] Department of Mechanical Engineering, Bahauddin Zakriya University, Multan, Pakistan

Original scientific paper
https://doi.org/10.2298/TSCI210402307H

The rapid development in the field of electronics has led to high power densities and miniaturization of electronic packages. Because of the compact size of electronic devices, the rate of heat dissipation has increased drastically. Due to this reason, the air-cooling system with a conventional heat sink is insufficient to remove large quantity of heat. A novel macro-channel 'L-shaped heat sink' is proposed and analyzed to overcome this problem. The thermal resistance and fluid-flow behavior under natural convection, of the novel and conventional air-cooled heat sink designs, are analyzed. Governing equations are discretized and solved across the computational domain of the heat sink, with 3-D conjugate heat transfer model. Numerical results are validated through experimentation. The effect of parameters i.e., fin height, number of fins and heat sink size, on the thermal resistance and fluid-flow are reported. Examination of these parameters provide a better physical understanding from energy conservation and management view point. Substantial increase in the thermal performance is noted for the novel 'L-shaped heat sink' compared to the conventional design.

Key words: *heat Sink, L-shape heat sink, novel design, thermal management, thermal analysis, heat transfer*

Introduction

In modern electronic systems, excessive heat is generated in PCB due to compact designs of the electronic chips. The heat generated in chip, decrease life of the electronic devices; hence, proper thermal management is needed to reduce temperature. For that purpose, aluminium heat sinks are used both in active and passive cooling systems to efficiently transfer heat between ambient air and electronic package. Heat transfer is dependent on the contact area between two heat exchanging materials. In this case, many vertical plates (according to design) are mounted on the horizontal plate which act as a base, to increase contact area. Due to the heat transfer efficiency, simple geometry and low manufacturing cost, a conventional heat sink with plate fins are most commonly used. A lot of studies have been reported on plat fin heat sinks to optimize various parameters and study thermal characteristics. Jones and

* Corresponding author, e-mail: m.siddiqi5@aston.ac.uk

Smith [1] studies conventional heat sink with straight fins and found that spacing between two consecutives fins is the important geometric parameter. They also concluded that optimal fin spacing has relation with temperature difference and fin height for the same length of fins. Bar-Cohen [2] carried out experimentations to investigate optimum fin thickness. They found that optimum fin thickness varies with each individual combination of material, environmental and geometric constrains. Teertstra *et al.* [3] presented analytical model for forced convection in air cooled, conventional heat sinks. They claimed, that analytical model could be used to calculate the average heat transfer rate for electronic applications to select the appropriate heat sink according to the specifications. Baskaya *et al.* [4] numerically investigated the effect of fin height, fin spacing and temperature deference on heat transfer and observed that heat transfer is improved with increase in fin height. Also, de Lieto Vollaro *et al.* [5] numerically investigated parameters of plate fin array in vertical direction as a function of emissivity, thermal conductivity, dimensions and other properties of working fluid. Further, researches [6-8] carried out experimentation and observed the relation of fin height, fin length, fin orientation, and inter fin spacing with average heat transfer through natural convection in plate fin heat sinks and suggested correlations.

Numerical and experimental study is carried out by Shen *et al.* [9] and studied the effect of orientation on heat transfer rate using natural convection in conventional heat sinks which is used commonly, and suggested correlations for numerous Reyleigh numbers and orientations ($\mathrm{Nu} = C\mathrm{Ra}^m$). Considering the fact by Naik *et al.* [10], that in most cases heat sinks are placed in closed enclosures in electronic devices and experimentally observed the heat transfer rate through conventional heat sink placed in horizontal orientation below an adiabatic wall, through natural convection. They disclosed that increase in clearance between top shroud and heat sink eventually increase the average heat transfer coefficient.

Numerous designs and fin modifications have been proposed in past to improve heat transfer from the chip to ambient air, such as slope plat fins [11], perforated pin fins [12], plate pin fins with non-rectangular cross-sections [13], arrays of plate fin arranged in circle [14-18], and metal foams [19-21]. Natural convective heat transfer performance was studied by Kim *et al.* [13] for different cross-section of the vertical plate fins. Ledezma and Bejan [11] proposed sloped plate fins for the enhancement of overall heat transfer coefficient. Further, radial heat sink was optimized by Jang *et al.* [16] with respect to the height of the fin to reduce the mass and thermal resistance. Improved procedure was introduced by Costa and Lopes [14] to acquire specified cooling with minimum mass and material usage. Jang *et al.* [15] and Li *et al.* [17] incorporated a chimney in radial plate fin heat sink and investigated improvement in heat transfer rate. Further, hollow pin fin with circular profile was proposed by Elshafei [12] and found that heat transfer rate was better as compared to the solid fins. Filomeno *et al.* [22] performed numerical simulations on pin fin heat sink and proposed analytical model. Further, Taheri *et al.* [23] proposed a new liquid cooled heat sink design and compared with the conventional heat sink. They found that the thermal resistance reduced drastically. To increase the conductivity of the fluid highly conductive nanoparticles were mixed with the liquid [24-26].

Researchers in fast proposed many designs and carried out numerous simulations and experimentations to improve heat sink efficiency. However, no study has been reported on *L*-shaped fins heat sink. In the current study, a novel *L*-shape fin heat sink with simple geometry is proposed for the enhancement of convective heat transfer rate. Simulations are carried out considering natural convection and validated through experimental data. Convective heat transfer and air flow distributions of plate-fin heat sinks and proposed L-shape fin heat

sink are comparatively studied to reveal the benefits of the proposed heat sink's design. The current study focused on improving convective heat transfer coefficient by overcoming the air flow defects of widely used conventional flat fin heat sink.

Mathematical model description

Governing equations

For 3-D laminar flow, the momentum, continuity and thermal energy equations can be demonstrated [27]:

– energy equation

$$\rho C_p\left(u\frac{\partial T}{\partial x}+v\frac{\partial T}{\partial y}+w\frac{\partial T}{\partial z}\right)=k\left(u\frac{\partial^2 T}{\partial x^2}+v\frac{\partial^2 T}{\partial y^2}+w\frac{\partial^2 T}{\partial z^2}\right) \tag{1}$$

– momentum equations

$$\rho\left(u\frac{\partial u}{\partial x}+v\frac{\partial u}{\partial y}+w\frac{\partial u}{\partial z}\right)=-\frac{\partial_p}{\partial x}+\mu\nabla^2 u \tag{2}$$

$$u\frac{\partial v}{\partial x}+v\frac{\partial v}{\partial y}+w\frac{\partial v}{\partial z}=v\nabla^2 v+\mathrm{g}\beta\ (T-T_\infty) \tag{3}$$

$$\rho\left(u\frac{\partial w}{\partial x}+v\frac{\partial w}{\partial y}+w\frac{\partial w}{\partial z}\right)=-\frac{\partial_p}{\partial x}+\mu\nabla^2 w \tag{4}$$

– continuity equation

$$\frac{\partial u}{\partial x}+\frac{\partial v}{\partial y}+\frac{\partial w}{\partial z}=0 \tag{5}$$

where ρ is the fluid density, x, y, z – the directions, u, v, w – the velocities, C_p – the heat capacity, β – the thermal expansion coefficient, T – the surface temperature, T_∞ – the ambient temperature, and k – the thermal conductivity of conservation. Heat loss due to radiation in the current study is neglected [28].

The convective heat transfer and thermal resistance are calculated through the following equations.

– convective heat transfer coefficient equation [29]

$$h_{av}=\frac{Q}{A(T_s-T_a)} \tag{6}$$

– convective thermal resistance equation

$$R_{\mathrm{conv}}=\frac{1}{Ah} \tag{7}$$

where A is the total surface area of fins and base plate and h – the local convective heat transfer coefficient.

Power input to the heater is calculated through the following equation:

$$P_{\mathrm{in}}=IV \tag{8}$$

where P_{in} is the power input to the heater, I – the current, and V – the voltage.

Boundary conditions

To solve the governing equations, the following boundary conditions are considered for the current study.

At $x = 0$, inlet gauge pressure with uniform distribution was applied, where:

$$T_f = T_{in} = 273\text{K} \tag{9}$$

$$p = p_{in} = 0 \tag{10}$$

Ambient temperature of the working fluid (air) was considered 293 K (T_{in} = 273 K). Same boundary conditions are applied at the outlet of the domain at x = 1200.

Constant value of power was applied on the bottom surface of the sink, where:

$$y = 0 : -k_s \frac{\partial T_s}{\partial y} = q \tag{11}$$

and $q = 20 - 60\text{W}$.

All walls of the fluid domain are considered adiabatic except inlet and outlet boundaries, so that no loss of heat occurs through the walls:

$$\frac{\partial T_s}{\partial y} = \frac{\partial T_s}{\partial z} \tag{12}$$

Numerical model description

Computational domain set-up

The treated problem was a 3-D horizontal straight and *L*-shape finned heat sinks with different configurations shown in tab. 1. The computational domain with length, width and height of 1200 mm, 120 mm, and 120 mm, respectively, was taken as shown in fig. 1. According to the experimental set-up, two side of the domain (120 mm × 120 mm) were taken as opening. However, the remaining four sides were taken as insulated walls and no heat can escape. Heat sinks are placed in the center of domain with two different configurations, conventional heat sink with straight fins and proposed heat sink with *L*-shape fins, as shown in fig. 2. The thickness of the fins was considered constant and was 2 mm in the current study. However, the height of fins was taken 10 mm, 20 mm, and 30 mm to predict effect of fin height on heat transfer rate. Properties of the considered heat sink and air is shown in tab. 2. In the current study constant ambient temperature of 300 K was considered. Three different input powers are applied to the base of heat sink (20 W, 40 W, and 60 W).

Table 1. Factors and levels for simulation

Factors	Level 1	Level 2	Level 3
Heat sink shape	Conventional	*L*-shape	–
Heat sink size [mm]	50	70	90
Number of fins	5	7	9
Height of fin [mm]	10	20	30
Input power [W]	20	40	60

Table 2. Thermophysical properties of heat sink and air [27]

Property	Heat sink	Ambient air
M [kgms^{-1}]	Conventional	*L*-shape
Cn [Jkg^{-1}K^{-1}]	870	1000
P [kgm^{-3}]	2700	1.225
K [Wm^{-1}K^{-1}]	200	0.0242

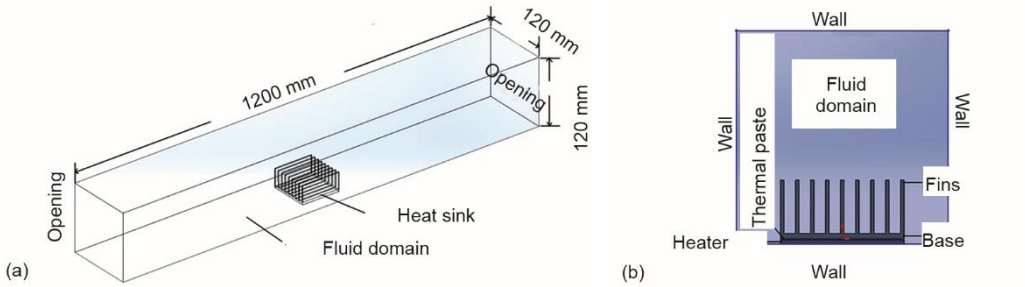

Figure 1. Computation domain

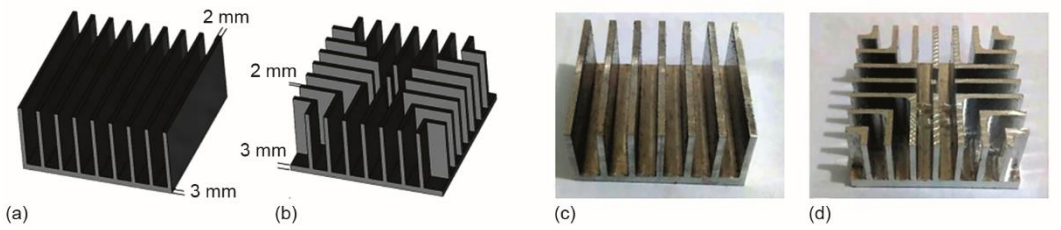

Figure 2. Geometry of (a) model of conventional heat sink, (b) model of L-shaped heat sink, (c) fabricated conventional heat sink, and (d) fabricated L-shape heat sink

Numerical procedure

The CFD software FLUENT 15 was used to solve the set of previous governing equations. First order discretization scheme is used to solve momentum and energy equations. Boussinesq approximation was used to approximate solution for natural convection problem dealt in this study. Standard scheme and SIMPLE method were applied for pressure correction equation and pressure-velocity coupling. The under-relaxation factors for pressure correction, velocity component and thermal energy were taken 0.3, 0.7, and 1, respectively. Convergence criterion for the solution was set to 10^{-6} for continuity and momentum and 10^{-9} for energy equation. Serial processing by i5 computer with 2.5 GHz Intel processors and 8 GB of RAM was used to run simulations. Each run took about six hours to converge solution.

Mesh independency test

Mesh independence test was carried out to choose suitable number of elements for an accurate simulation results. Different gird sizes are tested with different elements number to check the mesh independency of solution based on comparison of average temperature. Tests were performed with element numbers ranging from 325344 to 1119136 at 20 W power

input. Relative percent error (E%) was calculated for any M, between two mesh numbers (M1 and M2):

$$E\% = \left[\frac{M_2 - M_1}{M_1}\right]100 \tag{13}$$

Table 3. Mesh independency test

Number of	Number of	ΔT	E%
1	325344	54.81	3.61
2	476940	52.83	2.52
3	518208	51.5	1.55
4	665010	50.7	1.18
5	823480	50.1	0.40
6	922032	49.9	0.20
7	1119136	49.8	–

Relative error for ΔT is presented in tab. 3. It was observed that at 0.8 million and above the relative percent error was less than 0.5% for temperature deference and M5 is adequate for the simulation in current study.

Model validation

Model used in the current study is validated through experimentation on the bases of heat transfer coefficient. As shown in figs. 3 and 4, a slight difference below 9% was observed between numerical and experimental results. The difference could be due to the uncertainties in the measuring devices and the power supply to the heater. Further, in numerical simulation walls of the computational domain was taken as completely insulated (adiabatic), while in experimentation heat was lost to the environment through walls. However, numerical results show good agreement with experimental results. Thus, the model can be used for thermal analysis in the current study.

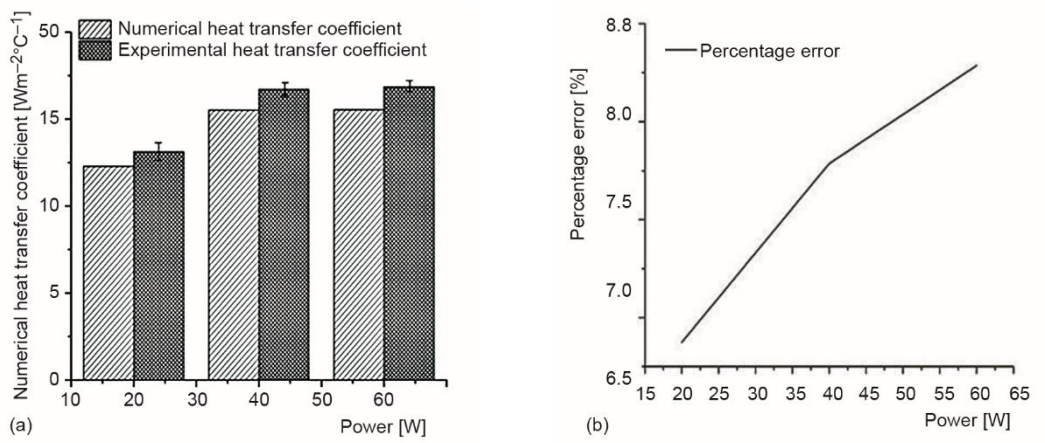

Figure 3. Model validation graph for conventional heat sink; (a) heat transfer coefficient and (b) percentage error

Experimental set-up and uncertainties

The TH320 free and forced convection apparatus was used to carry out experimentation in the current study as shown in fig. 5. Various instruments were used to measure input power to the heater, ambient temperature and temperature at different points of the heat sink, including fins and base.

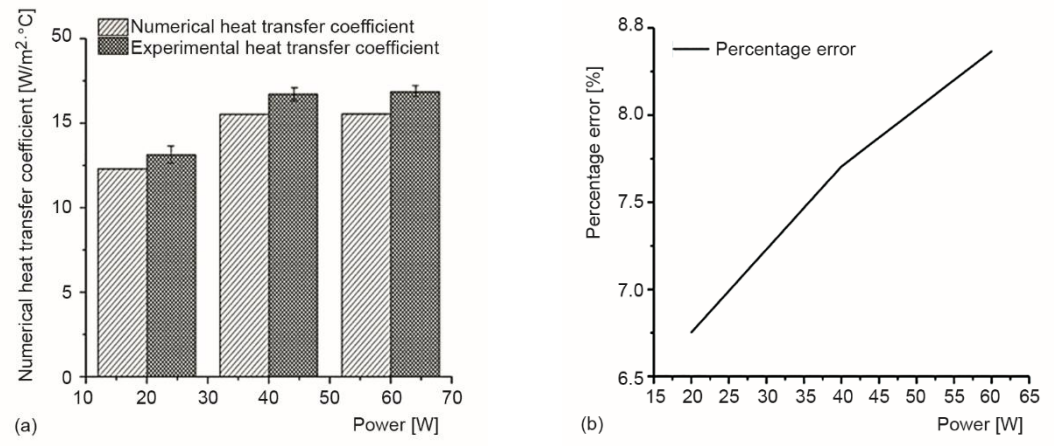

Figure 4. Model validation graph for *L*-shape heat sink; (a) heat transfer coefficient and (b) percentage error

Schematic of the experimental set-up is demonstrated in fig. 6. Heater was mounted to the bottom surface of the heat sink base to provide Dirichlet boundary condition. Thermal paste was used between the gape of heat sink and heater to ensure complete heat transfer to the heat sink base without heat loss. Rock wood insulation material was placed on lower surface of the heater to prevent heat loss. Five *K*-type thermocouples were placed on different positions of heat sink to find average temperature and one thermocouple is used to find ambient air temperature. Physical thermal data was recorded through TC-08 Data acquisition system and laptop. Power input to the heater was controlled using the power knob in control unit.

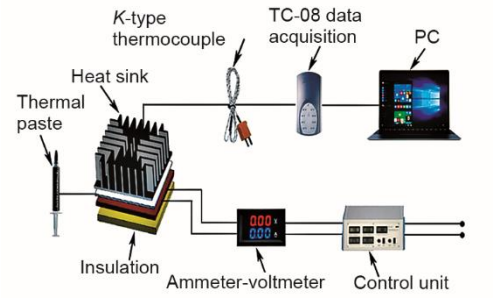

Figure 5. Schematic of the experimental set-up

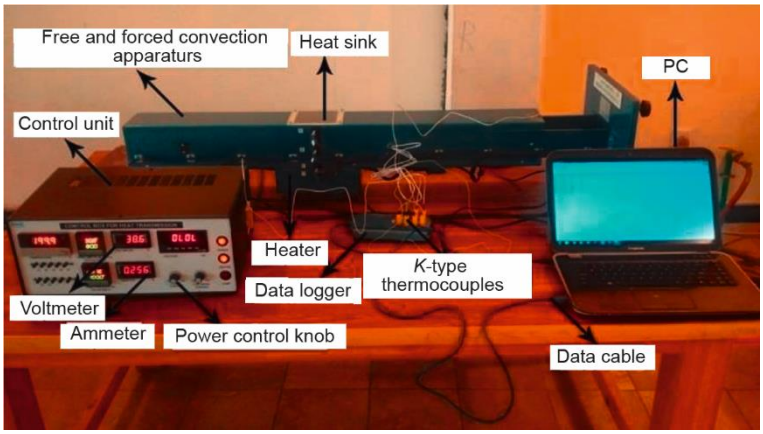

Figure 6. Experimental set-up for the current study experimentation

The experiments were carried out at constant room temperature in laboratory without any heating ventilation and air conditioning system. Accurate power input was feed to the 320 W heater using variable transformer in control unit. Input power of 20 W, 40 W, and 60 W were feed to the heater by varying voltage and current values. A voltmeter-ammeter was used to monitor voltage drop and current flow in order to calculate power input (power supplied = current flow × drop in voltage). Steady-state condition was assumed to be reached when temperature difference in each thermocouple is less than 0.5 °C per hour. Data was recorded after steady-state condition confirmation. Each experiment is repeated three times to ensure accurate readings.

The observed heat sinks configurations as well as geometrical parameters are shown in fig. 2. Heat sinks examined in the current study was manufactured from aluminum alloy 6063 which is commonly used in heat sink manufacturing and has 200 W/mK thermal conductivity. Denotations and dimensions of the two different configurations heat sinks studied experimentally are demonstrated in tab. 4. Length and width of the single heater was 100 mm × 100 mm. The number of fins for both conventional and proposed heat sink is taken 9. Height of the fins is taken 20 mm and base of the sink is considered 3 mm.

Table 4. Configuration for studied heat sinks

Fin type	Fin shape	Fin spacing [mm]	Fin height	Heat sink size [mm]
Type 1	Conventional	6	20	50
Type 2	*L*-shape	6	20	50

Total uncertainty, *U*, was estimated for the current set-up using error theory, which is the sum of uncertainties from various experimental apparatus that effect the experimental result. Considering the value of M, the results are a function of estimates $x1$, $x2$, $x3$, …, xN. To acquire standard measurement uncertainty, the standard uncertainty should be combined appositely for mentioned input estimates. To approximate M, the combined standard uncertainties are designated by *U* and the following equations are used for its calculations [30]:

$$\mathrm{M} = f(x1, x2, x3, ..., xN) \tag{14}$$

$$U(\mathrm{M}) = \left\{ \sum_{i=1}^{N} \left[\frac{\partial f}{\partial x_i} U(x_i) \right]^2 \right\}^{\frac{1}{2}} \tag{15}$$

where in terms of input estimates $x1$, $x2$, $x3$, …, xN, f is the function of M. Each $U(x_i)$ is the uncertainty of the independent variable x_i.

Both electrical parameters voltage, *V*, and current, *I*, are measured in the current study to calculate power input to the heater using eq. (8).

According to the manufacturers, reading accuracy for voltage and current values are 0.1%. Using the uncertainty concept in [31], eqs. (16) and (17) can be used to calculate measurement uncertainties [32]. Radiation effect is assumed to be neglected in the current study; hence, input heat can be assumed to be equal to heat transfer rate [33]:

$$\frac{\Delta P_{\text{in}}}{P_{\text{in}}} = \frac{\Delta q_{\text{in}}}{q_{\text{in}}} = \sqrt{\left(\frac{\Delta V}{V}\right)^2 + \left(\frac{\Delta I}{I}\right)^2} \tag{16}$$

$$\frac{\Delta R}{R} = \frac{\Delta q_{\text{in}}}{q_{\text{in}}} = \sqrt{\left(\frac{\Delta q}{q}\right)^2 + \left[\frac{\Delta(\Delta T)}{T}\right]^2} \tag{17}$$

Putting current, I, and voltage, V, values in eq. (8) results in maximum uncertainty of 6% for power input, P_{in}, which is equal to heat transfer rate, q. For temperature measurement, ΔT, the uncertainty is 1.1 K. Accuracy of thermocouples is also 1.1 K. Uncertainty in thermal resistance, R, is shown in the experimental results using error bars. Uncertainties along with the working ranges of the instruments used in the experimentation are listed in tab. 5. Average experimental uncertainties for the thermal resistances are estimated to be ±3.5%.

Table 5. Accuracy and working ranges of measuring devices

Description	Model	Range	Accuracy
Surface temperature	*K*-type	0-500	±1.1 K
Ambient temperature	*K*-type	0-500	±1.1 K
Ampere measurement	MT4W	0-500	±0.1 A
Voltage measurement	MT4W	0-5	±0.1 V
Length measurement	Calliper	6	±0.001 m

Results and discussion

Design evaluation

The conventional design has vertical straight fins in one direction, which allow the air to penetrate into heat sink from two sides. Air-flow across the straight fins was blocked by the horizontal fins, because there were no serrations that allows the air to enter from the other two sides of the heat sink as shown in fig. 7. However, in proposed design there are channels in all four directions which leads the air to flow from the edges to the center of the heat sink as shown in fig. 2. Square fin in the center, directs the hot air upward which promote natural circulation of air. Suction force produce due to the natural circulation forced ambient air to flow inside the channels to the center of the heat sink. Air-flow through the channels collide with perpendicular walls which further increase the heat transfer rate.

Closely observing the velocity contours and vectors in *X-Y* Plane for both conventional and *L*-shape heat sinks in fig. 8. The results revealed large central stagnation zone in conventional heat sink when compared to proposed heat sink, where small stagnation zone can be seen. The air movement was restricted in that zone, which results in high temperature as confirmed by the temperature contours in fig. 9. Though, heat transfer rate depends on temperature deference between surface and air temperature, the heat transfer rate decreases in stagnation zones. Furthermore, observing velocity vectors in *X-Y* for both heat sinks geometries, the velocity at channels inlet in conventional heat sink was much lower and in *L*-shaped geometry the velocity was comparatively high. Although, air velocity was directly related to Nusselt number which depicts maximum heat transfer rate with maximum velocity.

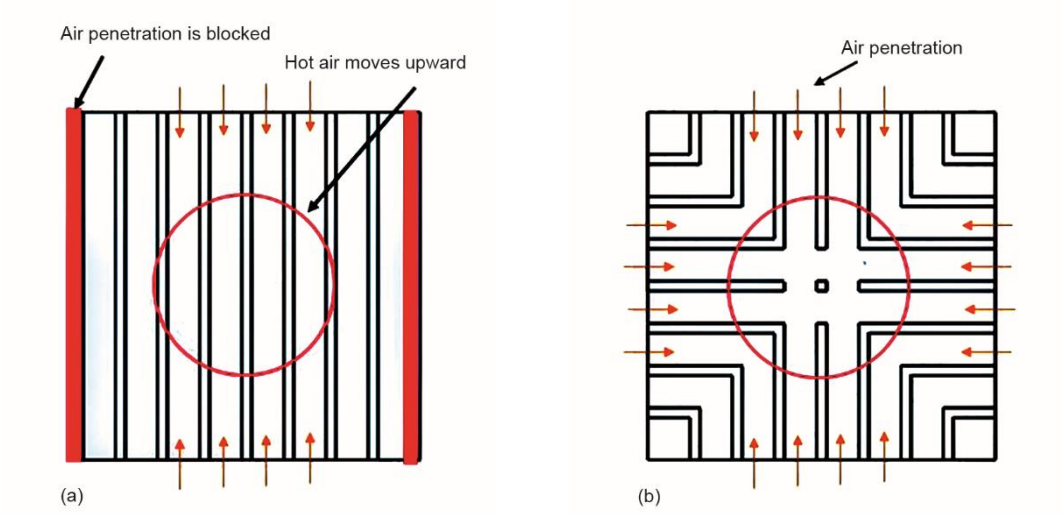

Figure 7. Air-flow in (a) conventional heat sink and (b) *L*-shape heat sink

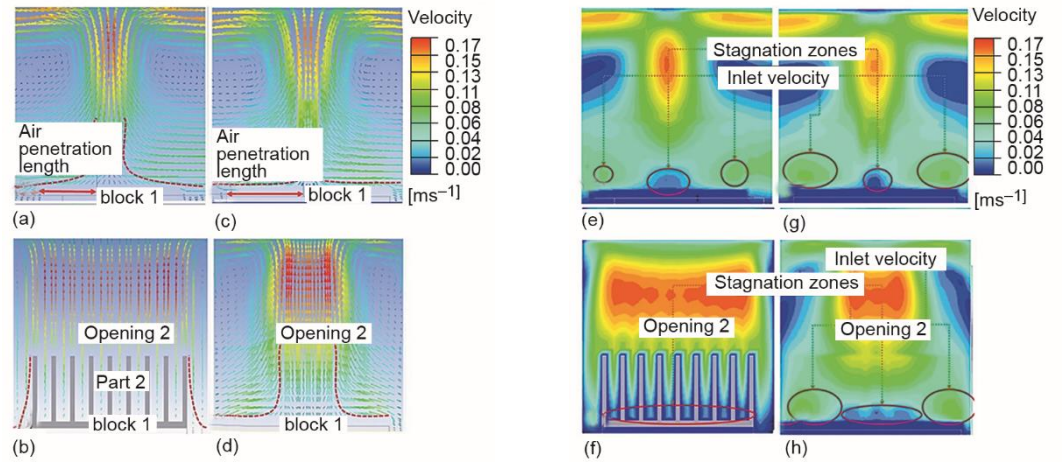

Figure 8. Air velocity vector for conventional heat sink; (a) *X-Y* plan, (b) *Y-Z* plan, air velocity vector for *L*-shape heat sink, (c) *X-Y* plan (d), *Y-Z* plan, air speed contours for conventional heat sink (e), *X-Y* plan, (f) *Y-Z* plan, air speed contours for *L*-shape heat sink, (g) *X-Y* plan, and (h) *Y-Z* plan
(*for color image see journal web site*)

Observing the temperature contours in fig. 9 confirms the phenomenon, as 39 °C temperature was noted on the channel inlet in *L*-shaped fins heat sink, while in conventional heat sink the temperature is 49 °C.

Analyzing the velocity vectors and contours in *Y*-Z plan in fig. 8 also disclosed interesting information about air-flow in both heat sink geometries. In straight fin geometry, local thermos-fluidic boundary was formed adjacent to the lower portion of the fins and heat sink base, which results in low local heat transfer rate. However, in the proposed geometry only in the center two small stagnation zones were appeared and was small comparatively. Figure 10 depicts the temperature distribution across the heat sinks in *X-Y* and *Y-Z* plan.

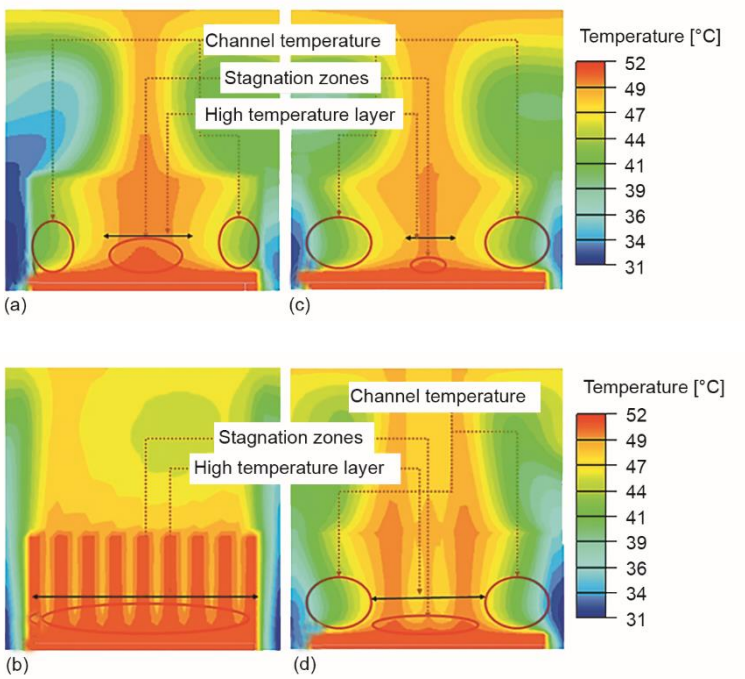

Figure 9 Air thermo-fluidic flow contours for conventional heat sink; (a) *X-Y* plan and (b) *Y-Z* plan and for *L*-shape heat sink (c) *X-Y* plane and (d) *Y-Z* plane
(*for color image see journal web site*)

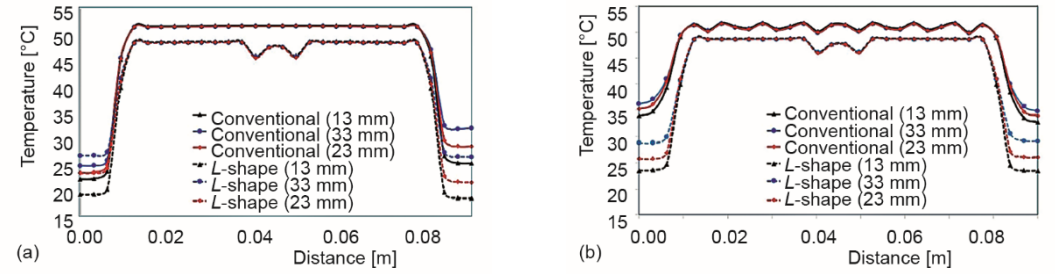

Figure 10. Comparison of thermal difference for conventional and *L*-shape heat sink; (a) *X*-direction and (b) *Y*-direction (*for color image see journal web site*)

Overall temperature in conventional heat was high with an average of 5 °C. Low temperature difference were seen between two geometries in *X*-direction, because both heat sinks permits air-flow in *X*-direction. However, low temperature in proposed heat sink geometry can be seen due to maximum penetration length of fresh air and comparatively high velocity on channel inlet. In addition to that, significant difference in *Y*-direction can be noted between the studied geometries. The observed difference was due to the fact, that proposed design also permits the air-flow in this direction. However, in conventional geometry the air-flow was blocked by the fins in the same direction.

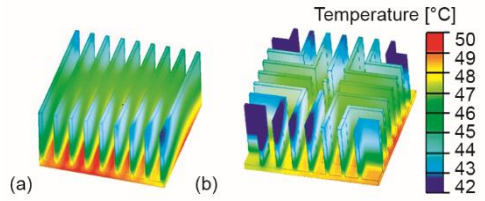

Figure 11. Surface temperature contours for; (a) conventional heat sink and (b) *L*-shape heat sink (*for color image see journal web site*)

Figure 11 shows the surface temperature contours of both heat sinks. It is clear that temperature of fins near the edges in all four sides was low because fresh air can penetrate in all four sides. However, in conventional heat sink low temperature of the fins can be seen in only two sides. Overall, the base temperature was lower in *L*-shape when compared to conventional heat sink.

Effect of input power

In this study thermal resistance was calculated for various combinations of input variables to predict heat transfer behavior in both heat sinks. Thermal resistance gives detailed insight of heat transfer rate from an electronic chip to an ambient air through heat sink. Efficient heat sinks allow maximum heat to transfer into surrounding, which results in low thermal resistance.

As shown in fig. 12, thermal resistance decreases for conventional heat sink and increases slightly for *L*-shape heat sink as the input power increases from 20-60 W. At high power, *i.e.* 60 W, the difference between thermal resistances of both heat sinks decreases significantly. However, maximum difference was observed at 20 W. High power results in high thermal density in chip, which produce maximum temperature difference between chip and ambient air and was accounts for maximum heat transfer. Closely observing the trends, *L*-shape heat sink show low thermal resistance when compared to the conventional heat sink.

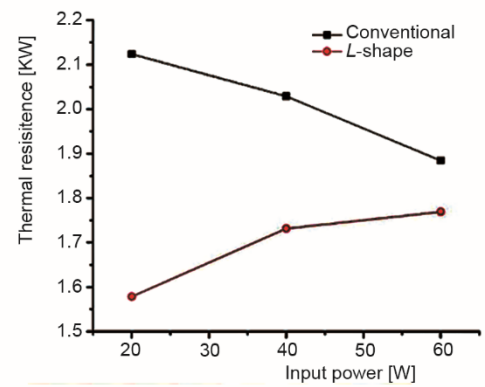

Figure 12. Effect of input power on thermal resistance

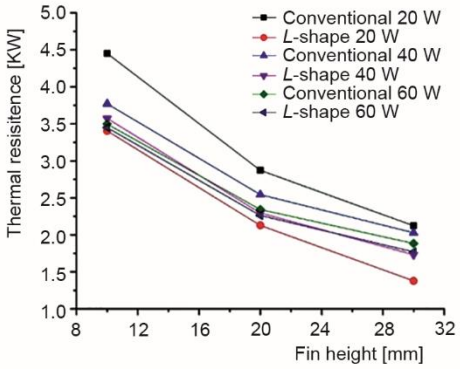

Figure 13. Effect of fin height on thermal resistance

Effect of fin number

Effect of fin numbers on heat transfer coefficient is illustrated in fig. 13. It was observed that thermal resistance decreases gradually for both heat sinks when number of fins increases for all input powers. Dramatic decrease can be observed for both heat sinks and all input powers when fin numbers increase from 5-7. However, further increase in fin numbers accounts for slight decrease in thermal resistance. This was due to the fact that increase in fin numbers reduces pitch length (inter fin distance) which resist air flow due to fraction as shown in speed contours in fig. 8. The loss in air velocity accounts for minimum heat transfer

which resulted in high thermal resistance. Overall, thermal resistance was low in *L*-shape heat sink when compared to convention heat sink. This improvement was caused by the air collision perpendicularly with fins in the corner of *L*-shape fins.

Effect of fin height

Thermal resistance decreases significantly when extended fins height increases for both type of heat sinks as depicted in fig. 14. It was due to the increase of surface area of the heat sink as extra material was added to the fins. As shown in eq. (6), heat transfer rate depends of surface area. Both heat sinks trend shows same behavior with all input power. However, difference between both the heat sinks decreases when input power rises from 20-60 W. Overall, the results show low thermal resistance for *L*-shape heat sink when compared to the thermal resistance of that of the conventional heat sink.

Effect of heat sink size

Effect of heat sink size on thermal resistance also show decreasing trend as shown in fig. 15. Sharp declination can be seen in the trend lines for both the heat sinks as heat sink size increase from 50-90 mm for the input power of 20 to 60 W. Decrease in thermal resistance occurred due increase in surface area. Overall, *L*-shaped heat sink performed well when compared to conventional heat sink, as the thermal resistance was low.

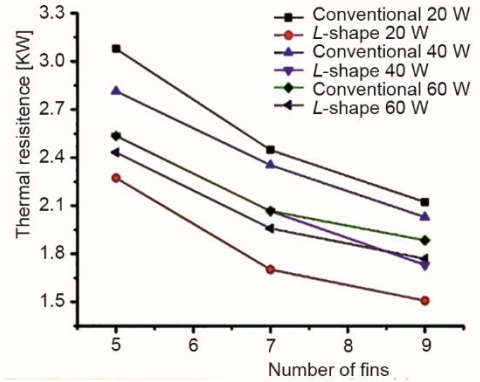

Figure 14. Effect of fins number on thermal resistance

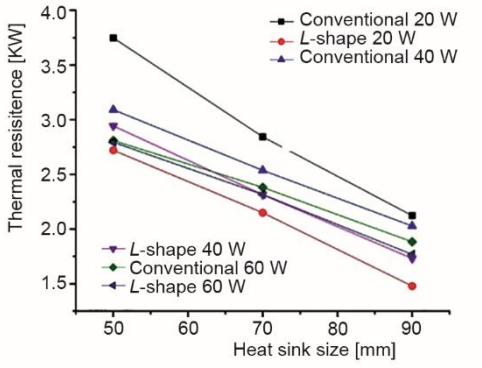

Figure 15. Effect of heat sink size on thermal resistance

Conclusion

A new *L*-shape heat sink was designed and manufactured, which comprised of *L*-shaped fins. An experimental and numerical study was carried out to measure the thermal resistance of both the conventional and proposed heat sink under natural convection. Moreover, experimentation was done and found good agreement between experimental and numerical results. Results obtained for *L*-shaped geometry in terms of thermal resistance, R_{th}, was compared with conventional heat sink. Based on obtained results following conclusions are drawn:

- In the *L*-shaped fin heat sink, open channels in all four sides enhances the fluid-flow and eventually increases the heat transfer rate.

- It is also interesting to note that an average of 12.35% enhancement in thermal resistance, R_{th}, is observed when proposed heat sink is compared to the commonly used conventional heat sink.
- The results revealed that heat sink size, fin height and _n numbers have significant inverse relation with thermal resistance, R_{th}.
- The square fin in the center of proposed heat sink accelerate and direct the hot air to produce strong vacuum, which forces the fresh air to penetrate to the center of the heat sink and contribute to high heat transfer rate, hence decreases thermal resistance.
- For the studied heat sink, heat sink with 30 mm fin height, 90 mm by 90 mm heat sink size and 9 fin numbers have minimum thermal resistance, R_{th}, and can be considered as the optimal design for the proposed design.
- Overall, comparing the proposed heat sink with conventional heat sink on the bases of thermal resistance and fluid ow and temperature contours, the proposed design has better heat transfer rate.

References

[1] Jones, C. D., Smith, L. F., Optimum Arrangement of Rectangular Fins on Horizontal Surfaces for Free-Convection Heat Transfer, *Journal of Heat Transfer, 92* (1970), 1, pp. 6-10
[2] Bar-Cohen, A., Fin Thickness for an Optimized Natural Convection Array of Rectangular Fins, *Journal of Heat Transfer, 101* (1979), 3, pp. 564-566
[3] Teertstra, P., *et al*., Analytical Forced Convection Modeling of Plate Fin Heat Sinks, *Journal of Electronics Manufacturing, 10* (2000) 4, pp. 253-261
[4] Baskaya, S., *et al*., Parametric Study of Natural Convection Heat Transfer from Horizontal Rectangular Fin Arrays, *International Journal of Thermal Sciences, 39* (2000), 8, pp. 797-805
[5] de Lieto Vollaro, A., *et al.*, Optimum Design of Vertical Rectangular Fin Arrays, *International journal of Thermal Sciences, 38* (1999), 6, pp. 525-529
[6] Mehrtash, M., Tari, I., A Correlation for Natural Convection Heat Transfer from Inclined Plate-Finned Heat Sinks, *Applied Thermal Engineering, 51* (2013), 1-2, pp. 1067-1075
[7] Tari, I., Mehrtash, M., Natural Convection Heat Transfer from Horizontal and Slightly Inclined Plate-Fin Heat Sinks, *Applied Thermal Engineering, 61* (2013), 2, pp. 728-736
[8] Tari, I., Mehrtash, M., Natural Convection Heat Transfer from Inclined Plate-Fin Heat Sinks, *International Journal of Heat and Mass Transfer, 56* (2013), 1-2, pp. 574-593
[9] Shen, Q., *et al*., Orientation Effects on Natural Convection Heat Dissipation of Rectangular Fin Heat Sinks Mounted on LEDs, *International Journal of Heat and Mass Transfer, 75* (2014), Aug., pp. 462-469
[10] Naik, S., *et al*., Natural-Convection Characteristics of a Horizontally-Based Vertical Rectangular Fin-Array in the Presence of a Shroud, *Applied Energy, 28* (1987), 4, pp. 295-319
[11] Ledezma, G., Bejan, A., Heat Sinks with Sloped Plate Fins in Natural and Forced Convection, *International Journal of Heat and Mass Transfer, 39* (1996), 9, pp. 1773-1783
[12] Elshafei, E., Natural Convection Heat Transfer from a Heat Sink with Hollow/Perforated Circular Pin Fins, *Proceedings,* 3rd International Conference on Thermal Issues in Emerging Technologies Theory and Applications, Cairo, Egypt, 2010, IEEE, pp. 185-193
[13] Kim, D. K., Thermal Optimization of Plate-Fin Heat Sinks with Fins of Variable Thickness Under Natural Convection, *International journal of Heat and Mass Transfer, 55* (2012), 4, pp. 752-761
[14] Costa, V. A., Lopes, A. M., Improved Radial Heat Sink for Led Lamp Cooling, *Applied Thermal Engineering 70* (2014), 1, pp. 131-138
[15] Jang, D., *et al*., The Orientation Effect for Cylindrical Heat Sinks with Application to LED Light Bulbs, *International Journal of Heat and Mass Transfer, 71* (2014), Apr., pp. 496-502
[16] Jang, D., *et al*., Optimum Design of a Radial Heat Sink with a Fin-Height Profile for High-Power LED Lighting Applications, *Applied Energy 116* (2014), Mar., pp. 260-268
[17] Li, B., *et al*., Enhanced Natural Convection Heat Transfer of a Chimney-Based Radial Heat Sink, *Energy Conversion and Management, 108* (2016), Jan., pp.422-428

[18] Park, S. J., *et al*., Optimization of a Chimney Design for Cooling Efficiency of a Radial Heat Sink in a LED Downlight, *Energy Conversion and Management, 114* (2016), Apr., pp. 180-187
[19] Bhattacharya, A., Mahajan, R. L., Metal Foam and Finned Metal Foam Heat Sinks for Electronics Cooling in Buoyancy-Induced Convection, *Journal of Electronic Packaging, 128* (2006), 3, pp. 259-26
[20] Feng, S. S., *et al*., An Experimental and Numerical Study of Finned Metal Foam Heat Sinks Under Impinging Air Jet Cooling, *International Journal of Heat and Mass Transfer, 77* (2014), Oct., pp. 1063-1074
[21] Feng, S., *et al*., Natural Convection in Metal Foam Heat Sinks with Open Slots, *Experimental Thermal and Fluid Science, 91* (2018), Feb., pp. 354-362
[22] Filomeno, G., *et al.,* Automatization of Pin Fin Heat Sink Design with Geometric and Fluid Constraints, *International Journal of Mechanical Engineering and Robotics Research, 9* (2020), 5, pp. 652-657
[23] Taheri, A., *et al.*, A New Design of Liquid-Cooled Heat Sink by Altering the Heat Sink Heat Pipe Application: Experimental Approach and Prediction Via Artificial Neural Network, *Energy Conversion and Management, 206* (2020), Feb., 112485
[24] Ghadikolaei, S., *et al.*, Fe_3O_4–(CH_2OH) 2 Nanofluid Analysis in a Porous Medium Under MHD Radiative Boundary Layer and Dusty Fluid, *Journal of Molecular Liquids, 258* (2018), May, pp. 172-185
[25] Amiri, A., *et al.*, Laminar Convective Heat Transfer of Hexylamine-Treated MWCNTs-Based Turbine Oil Nanofluid, *Energy Conversion and Management, 105* (2015), Nov., pp. 355-367
[26] AL-Musawi, A. I. A., *et al.,* Numerical Study of the Effects of Nanofluids and Phase-Change Materials in Photovoltaic Thermal (PVT) Systems, *Journal of Thermal Analysis and Calorimetry, 137* (2019), 2, pp. 623-636
[27] Mousavi, H., *et al*., A Novel Heat Sink Design with Interrupted, Staggered and Capped Fins, *International Journal of Thermal Sciences, 127* (2018), May, pp. 312-320
[28] Haghighi, S. S., *et al*., Natural Convection Heat Transfer Enhancement in New Designs of Plate-Fin Based Heat Sinks, *International Journal of Heat Mass Transfer, 125* (2018), Oct., pp. 640-647
[29] Yalcin, H. G., *et al*., Numerical Analysis of Natural Convection Heat Transfer from Rectangular Shrouded Fin Arrays on a Horizontal Surface, *International Communications in Heat Mass Transfer, 35* (2008), 3, pp. 299-311
[30] Rao, V. R., Venkateshan, S. P., Experimental Study of Free Convection and Radiation in Horizontal Fin Arrays, *International Journal of Heat and Mass Transfer, 39* (1996), 4, pp. 779-789
[31] Holman, J. P., *Experimental Methods for Engineers*, Mc Graw and Hill, New York, USA, 2001
[32] Goshayeshi, H. R., *et al*., Effect of Magnetic Field on the Heat Transfer Rate of Kerosene/Fe_2O_3 Nanofluid in a Copper Oscillating Heat Pipe, *Experimental Thermal and Fluid Science, 68* (2015), Nov., pp. 663-668
[33] Mostafavi, G., M. *et al.,* Effect of Fin Interruptions on Natural Convection Heat Transfer From a Rectangular Interrupted Single-Wall, *Proceedings,* International Electronic Packaging Technical Conference and Exhibition, Mani, Hi., USA, 2013

Paper submitted: April 2, 2021
Paper revised: May 16, 2021
Paper accepted: May 20, 2021